



**HAL**  
open science

## Supercritical Angle Fluorescence for Enhanced Axial Sectioning in STED Microscopy

Iván Coto Hernández, Siddharth Sivankutty, Iván Coto, Hernández 1+,  
Nicolas Bourg, Guillaume Dupuis, Sandrine Leveque-Fort

► **To cite this version:**

Iván Coto Hernández, Siddharth Sivankutty, Iván Coto, Hernández 1+, Nicolas Bourg, et al.. Supercritical Angle Fluorescence for Enhanced Axial Sectioning in STED Microscopy. *Methods*, 2019, 174, pp.20-26. 10.1016/j.ymeth.2019.03.027 . hal-02400230

**HAL Id: hal-02400230**

**<https://hal.science/hal-02400230>**

Submitted on 11 Dec 2020

**HAL** is a multi-disciplinary open access archive for the deposit and dissemination of scientific research documents, whether they are published or not. The documents may come from teaching and research institutions in France or abroad, or from public or private research centers.

L'archive ouverte pluridisciplinaire **HAL**, est destinée au dépôt et à la diffusion de documents scientifiques de niveau recherche, publiés ou non, émanant des établissements d'enseignement et de recherche français ou étrangers, des laboratoires publics ou privés.

# STED Microscopy with Nanometer Axial Sectioning

*Siddharth Sivankutty*<sup>1,+,#</sup>, *Iván Coto Hernández*<sup>1+</sup>, *Nicolas Bourg*<sup>1</sup>, *Guillaume Dupuis*<sup>2\*</sup>, and  
*Sandrine Lévêque-Fort*<sup>1,\*</sup>

<sup>1</sup> Institut des Sciences Moléculaires d'Orsay, CNRS, Univ. Paris-Sud, Université Paris-Saclay, F-91405, Orsay, France

<sup>2</sup> Université Paris-Sud, Centre de Photonique BioMédicale (CPBM), Fédération LUMAT, CNRS FR 2764, F91405 Orsay Cedex, France

<sup>+</sup> Both authors contributed equally to this work

<sup>#</sup> current address : Institut Fresnel , Aix-Marseille Université, CNRS, Centrale Marseille, UMR 7249, 13397 Marseille Cedex 20, France

\* corresponding authors: [guillaume.dupuis@u-psud.fr](mailto:guillaume.dupuis@u-psud.fr); [sandrine.leveque-fort@u-psud.fr](mailto:sandrine.leveque-fort@u-psud.fr)

## Abstract

We demonstrate subwavelength axial sectioning on biological samples with a stimulated emission depletion (STED) microscope combined with supercritical angle fluorescence (SAF) detection. SAF imaging is a powerful technique for imaging the membrane of the cell based on the direct exploitation of the fluorophore emission properties. Indeed, only when fluorophores are close to the interface can their evanescent near-field emission become propagative and be detected beyond the critical angle. Therefore, filtering out the SAF emission from the undercritical angle fluorescence (UAF) emission in the back focal plane of a high-NA objective lens permits nanometric axial sectioning of fluorescent emitters close to the coverslip. When combined with STED microscopy, a straightforward gain in axial resolution can be reached without any alteration of the STED beam

1 path. Indeed, STED-SAF implementation only requires a modification in the detection path of the  
2 STED microscope and thus could be widely implemented.

3

#### 4 **1. Introduction**

5 Many biological studies require imaging with superior axial resolution to specifically target cell  
6 membrane processes [1,2] such as cell motility, adhesion or protein trafficking. However, the axial  
7 resolution of conventional fluorescence microscopy does not permit thin optical sectioning of the  
8 membrane from the volume of the cell. The improvement of the axial resolution has been a  
9 fundamental problem in optical microscopy. To date several progresses have been done to improve  
10 the lateral and axial resolution beyond the diffraction limit. However, isotropic resolution in all  
11 three dimensions is still a challenge in many superresolution techniques [3]

12 Circumventing the diffraction limit in fluorescence microscopy became possible by exploiting  
13 molecular transitions of the fluorophore [4]. For instance, one of the most popular cellular imaging  
14 techniques is stimulated emission depletion (STED) microscopy [5,6] known for its unprecedented  
15 spatial resolution. However, the axial resolution of a conventional STED microscope still remains  
16 similar to confocal microscopy and resolution enhancement [7,8] along the axial direction comes at  
17 the cost of complex instrumentation and the reduction of lateral resolution. Furthermore, 3D-STED  
18 requires a greater power for the STED beam, which can have negative consequences on the sample.  
19 In the specific case of membrane or flat-cells imaging, STED microscope has been coupled with  
20 Total Internal Reflection Fluorescence (TIRF) microscopy [9,10], which is based on evanescent  
21 excitation and provides subwavelength axial sectioning in the vicinity of the coverslip. However, it  
22 requires unconventional polarization states for the excitation beam [9] and suffers from the usual  
23 drawbacks of TIRF microscopy such as inhomogeneous illumination of the field of view and loss of  
24 axial confinement due to stray excitation [11]. More importantly, it requires a modification of the

1 excitation/depletion optical path, which can lead to a degradation of the lateral resolution.  
2 Regardless, evanescent waves do appear as an elegant method to produce axial sectioning. Here, we  
3 therefore propose to take advantage of evanescent waves from the detection point of view rather  
4 than from the excitation, and thus preserve the qualities of an optimized excitation/depletion optical  
5 path [12]. Our alternate approach to TIRF-STED microscopy consists in exploiting the supercritical  
6 angle fluorescence (SAF) emission of fluorophore (see Fig.1). It provides another way to achieve  
7 sub-diffraction axial sectioning by limiting detection to the immediate vicinity of the sample-  
8 substrate interface. Indeed, when a fluorophore is close to the glass/medium interface, the  
9 evanescent near-field components of its emission becomes propagative in the medium with a higher  
10 refractive index, which manifests as light emitted above the critical angle [13]. This SAF emission  
11 can represent up to 50% of the emission collected by the objective for a fluorophore located at the  
12 interface itself and sharply decreases when it is further away. The discrimination of the SAF  
13 components from the undercritical angle fluorescence (UAF) is the experimental key to achieve  
14 axial sectioning in a SAF-based imaging technique. Early implementations of this discrimination  
15 were based on a specifically designed objective lens that filtered the near-field components in the  
16 object space directly [14]. However, this approach is not applicable here since it would affect both  
17 the excitation and detection paths and would result in a degradation of lateral resolution. The recent  
18 wide dissemination of SAF microscopy came with the demonstration that SAF microscopy is  
19 possible by filtering out the SAF components by inserting a dedicated amplitude mask in the  
20 detection pathway of the microscope at a position conjugated with the back-focal plane of a high-  
21 NA objective lens [15]. This method reduces complexity and increases the portfolio of applications  
22 since filtering only occurs in the detection path while the excitation path requires virtually no  
23 modification whatsoever. It has been demonstrated as versatile because it has been implemented  
24 both in widefield [15,16] and confocal modes [17]. Recently, the benefits of SAF detection have  
25 been combined with Single Molecule Localization Microscopy (SMLM) to yield an almost  
26 isotropic three-dimensional localization precision better than 20 nm [18,19]

1 In contrast with SMLM, STED microscopy is faster and compatible with live cells imaging. This  
2 motivates us to combine the strengths of these two methods to open new perspectives for super-  
3 resolution imaging of thin samples [20]. Therefore, we report here a novel membrane-specific  
4 microscope, which takes advantage of supercritical angle emission (here onwards referred to as  
5 STED-SAF). Membrane-specific imaging is obtained without any change in the illumination path,  
6 simply by adding a SAF module in the detection path of any given STED microscope. This upgrade  
7 to STED microscopy enhances axial sectioning at the vicinity of the coverslip with no alteration of  
8 the excitation/emission path and will contribute to more applications of STED microscopy. We  
9 implemented a STED-SAF microscope compatible with green and yellow fluorescent dyes.  
10 However, the same performance can be tuned to other wavelengths or multicolor regimes without  
11 any increase in the architectural complexity.

12

## 13 **2. Materials and methods**

### 14 **2.1. STED-SAF instrumentation**

15 We implemented the STED microscope on top of an existing custom made confocal SAF  
16 microscope [17] based on a compact fiber-based supercontinuum (SC) source (SC450-HE,  
17 Fianium) that is adapted to the implementation of compact and tunable STED microscopes [21]  
18 with a wide choice of fluorophores (see Fig. 2). In the present configuration we set the wavelength  
19 of the excitation beam to  $\lambda_{\text{exc}} = 488 \pm 6$  nm necessary for applications requiring visible fluorescent  
20 proteins (such as GFP and YFP) while the depletion beam was set at  $\lambda_{\text{STED}} = 585 \pm 10$  nm. The use  
21 of the same laser for excitation and depletion reduces complexity and avoids problems with jittering  
22 or synchronization of the two lasers. We used two optical fibers to allow finer pulse-stretching to  
23 optimize the pulse width requirement and improve the beam quality. The low repetition rate of this  
24 laser (0.5, 1 or 2 MHz) significantly slows down the imaging speed but reduces photobleaching

1 [22,23]. The STED beam passes through a polymeric mask imprinting  $0-2\pi$  helical phase-ramps  
2 (VPP-A1, RPC Photonics) and is circularly polarized at the back-aperture of the objective lens by  
3 an achromatic quarter-wave plate (RAC 3.4.15, Bernhard Halle Nachfl.). The illumination beams  
4 are tightly focused on the sample with a 60x oil immersion objective lens with high numerical  
5 aperture (NA = 1.49). For 3D scanning of the sample we use a piezo-electric stage scanner (P-545)  
6 with a scan controller (E-710) from Physik Instrument. Using a stage scanner further improves the  
7 spatial resolution due to superior stability, nano-positioning and perfect overlap of the beams  
8 through the entire field of view. The fluorescence light is collected by the same objective lens and  
9 passes through the dichroic mirrors as well as through a fluorescence band pass filter (ET Bandpass  
10 525/50 nm, AHF analysentechnik).

## 11 **2.2. Optical alignments**

12 The imaging performance of the STED-SAF microscope crucially depends on two factors, i) the  
13 spatial overlap of the excitation and the STED beams on the sample plane and ii) the positioning of  
14 the amplitude mask on the conjugated back focal plane. We employed standard techniques of  
15 optical alignment initially to co-align the beams on to the optical axis of the microscope. In order to  
16 inspect the fine spatial overlap of the beams on the sample plane and the quality of the excitation  
17 and the doughnut-like STED PSF, we imaged a sample of gold nano spheres (100 nm) in a back-  
18 scattering configuration. We employed a thin pellicle beam splitter right below the microscope  
19 objective to ensure that part of the backscattered signal ( $<2\%$ ) from the beads was focused onto a  
20 photomultiplier tube (PMT, Hamamatsu) placed in a non-confocal configuration. Such an  
21 arrangement permitted the co-registration of the excitation and the STED beam by scanning the  
22 piezo-electric stage and allowed us to overlap the beams with a very high precision. This auxiliary  
23 system also allowed us to visually inspect the beam quality of both the beams, and thus provide a  
24 feedback to center and tilt the vortex phase mask for an optimal STED PSF.

1 For true comparison of STED-SAF with conventional STED the fluorescence signal is collected  
2 simultaneously into two confocal channels by a pellicle beamsplitter (BP145B1, Thorlabs). The  
3 specific collection of SAF emission was possible by inserting a SAF detection module in one of the  
4 two detection paths of our STED microscope. This module relies on a telescope with x1.2  
5 magnification to access a plane conjugated with the back-focal plane of the objective lens where we  
6 placed a circular central amplitude mask (3.9-mm diameter) to block all the light emanating from  
7 under the critical angle. For the alignment of the SAF module, after an initial Koehler alignment of  
8 the conventional white light illumination on the microscope, we coarsely identify the position of the  
9 conjugate aperture stop on the detection channel. A flip-mirror placed downstream and an imaging  
10 system equipped with a Bertrand lens ( $f = 150$  mm), allows us to image this plane on to a CCD  
11 camera (ORCA 4.0, Hamamatsu). For fine alignment, we then use a sample of 100 nm fluorescent  
12 beads (Yellow-Green, Invitrogen) and adjust the axial position of the camera such that the  
13 characteristic concentric pattern associated with UAF and SAF fluorescence emission is imaged  
14 crisply. Using this system, the size of the amplitude mask is verified, and its position is carefully  
15 adjusted and centered such that only the SAF components are visible and all the UAF components  
16 are blocked. After these alignments, both the pellicle beam-splitter below the microscope objective  
17 and the flip mirror is removed during the image acquisition.

### 18 **2.3. STED-SAF acquisition**

19 Both channels are focused (focal length 150 mm, AC254-150-A-ML, Thorlabs) into two fiber-  
20 pigtailed single photon avalanche photodiodes (SPAD, Picoquant). The graded index multimode  
21 fiber with 62.5  $\mu\text{m}$  and 102.5  $\mu\text{m}$  cores respectively of the SPAD acted as confocal pinholes of 1.2  
22 and 2.4 times the size of the projected Airy disk at 520 nm. To control the image acquisition we  
23 used a time-correlated-single-photon-counting-card (TCSPC) (HydraHarp 400, PicoQuant),  
24 synchronized with the reference signal provided by the Fianium laser and a trigger signal from the

1 scanning system. All imaging operation and analysis was automated and managed by the software  
2 SymPhoTime 64 (SPT64, version 2.1, PicoQuant).

## 3 **2.4. Sample preparations**

### 4 **2.4.1. PSF measurements**

5 The experimental PSF of the instrument is obtained by imaging fluorescent 40-nm latex beads (~ 40  
6 nm diameter, Yellow-Green, Invitrogen). We diluted the fluorescent beads in phosphate-buffered  
7 saline (PBS) by 1:3000 (v/v), we dropped 1mL of the diluted solution onto a glass coverslip placed  
8 in an open-bath imaging chamber and we waited 15 min for deposition of the beads on the  
9 coverslip.

### 10 **2.4.2. Immunofluorescence assays**

11 COS-7 cells (derived from monkey kidney tissue) are plated overnight on 18 mm diameter glass  
12 coverslips (No 1.5 ideal for superresolution) in DMEM supplemented with 5% FBS. The day after,  
13 the culture medium was removed and cells were immediately rinsed three times the cells in PHEM  
14 1X (37° C) for 5 min before being incubated for 10 min in paraformaldehyde (4%), glutaraldehyde  
15 (0.02%) in PHEM and 0.5% Triton for 20 min at room temperature. After fixation, the cells were  
16 washed three times in PBS (0.1 M, pH 7.4) and one time in Triton (0.1%) for 7 and 10 min  
17 respectively. Cells are then washed in PBS and incubated for 20 min in NaBH<sub>4</sub> (1 mg / ml) solution  
18 for reduction. Later, it was rinsed three times in PBS (0.1 M, pH 7.4) and rinsed again three times in  
19 PBS+ 1% BSA for 5 min for saturation. The cells were then incubated with the monoclonal mouse  
20 anti- $\alpha$ -tubulin antiserum (Sigma Aldrich) diluted (1:1000) in a blocking buffer (PBS + 1% BSA) for  
21 1 h at 37 ° C. The cells were rinsed three times in PBS for 5 min. The  $\alpha$ -tubulin antibody was  
22 revealed using Alexa Fluor 488 goat anti-mouse IgG (1:500, Molecular Probes in PBS + 1% BSA)  
23 for 45 min at 37° C and protected from light. After three washes in PBS, cells were rinsed in 3.6%  
24 formaldehyde in PBS during 16 min for post fixation. Cells are then washed three times in PBS for

1 5 min and rinsed during 10 min in NH<sub>4</sub>Cl (50 mM) in PBS for reduction. Finally the cells were  
2 washed in PBS and initially mounted on a coverslip and placed in an open-bath imaging chamber  
3 with an aqueous medium such as PBS. For STED-SAF imaging better results were found with a  
4 mount liquid antifade (4-0100-005-0, Abberior) with refractive index close to that of many  
5 biological samples (n=1.38), and lower than refractive index of glass to allow propagation and  
6 collection of SAF signal. Depending on the use of either PBS or a given mounting medium with a  
7 different refractive index, the size of the amplitude mask needed to be changed and adapted to the  
8 corresponding UAF/SAF distribution.

9

### 10 **3. Results and discussion**

#### 11 **3.1. Calculation of the molecular collection efficiency**

12 Using our previous work in confocal-SAF instrumentation [17], we simulated the molecular  
13 collection efficiency (MCE) for various experimental configurations to characterize the  
14 performance of our STED-SAF microscope in terms of lateral resolution and sectioning. In  
15 conventional STED imaging, the effective PSF in the observed superresolved image assuming no  
16 detection pinhole can be described as:

$$17 \quad h_{eff}(r, z) = h_{conf}(r, z) \times h_{STED}(r, z) \times \eta(I_{STED}(r, z)) \quad (1)$$

18 where  $h_{conf}(r, z)$  is the confocal PSF,  $h_{STED}(r, z)$  is the depletion PSF and  $\eta$  describes an exponential  
19 decrease of the spontaneous emission probability with the STED beam intensity. Physically this  
20 describes that the only the molecules that contribute to the image formation lies at the zeros of the  
21 STED beam. Similarly, we already reported the general theory governing confocal-SAF detection  
22 [17]: There exists an exponential dependence of the signal as a function of axial distance from the  
23 coverslip due to the evanescent decay of the near-field components. Hence, the MCE [24] is given  
24 as:

$$MCE(z) = \exp \frac{-z}{\delta z} \quad (2)$$

Therefore, we can model image formation in STED-SAF by accounting for both the spontaneous emission probability  $h_{eff}(r, z)$  and the MCE as:

$$Img_{STED-SAF}(r, z) = h_{eff}(r, z) * Obj(r, z) \times MCE(z) \quad (3)$$

Intuitively, this can be understood as follows: The probability that a molecule will contribute to the image drops exponentially with increasing power of the STED beam or as it moves away from the interface. The strong  $\sim 160$ -nm axial confinement obtained according to the theory is similar to the experimental value we previously reported (see Fig. 3). This axial sectioning is in the same order of magnitude as the  $\sim 100$ -nm axial resolution accessible with a 3D-STED microscope, though limited to the vicinity of the coverslip. The improved sectioning in SAF mode arises due to the rapid decay of the MCE when the axial position of the emitter is further away from the interface. This result regarding the axial confinement of the signal anticipates a strong enhancement compared with conventional STED microscope.

### 3.2. STED-SAF imaging

For validation of the results obtained in the simulation we performed some experiments on calibration and biological samples. We first imaged the microtubule network in fixed COS-7 cells immunolabeled with AF 488 in both confocal and SAF modes (see Fig. 4). In SAF mode, non-confocal detection presents the advantage of maximizing signal collection by avoiding signal loss at the pinhole. Besides out-of-focus fluorescence is inherently blocked by the central amplitude mask and we observed no degradation in the resolution. In the case of a more densely labeled sample, our previous results indicate that the use of a somewhat large pinhole does help reduce stray light from the system and improves contrast. In the case of the sample presented in Fig. 4, we can clearly see some features preserved in the SAF image while light from the volume of the cell is rejected. This underlines the improvement in axial sectioning permitted by SAF detection.

1 To highlight the benefits of STED-SAF microscopy, we imaged closely packed sub-diffraction  
2 sized (40 nm) yellow green fluorescence beads close to the surface (see Fig. 5) and compared  
3 confocal, confocal-SAF, STED and STED-SAF images. Beads that appear clustered together in  
4 confocal and SAF can be individually identified in STED and STED-SAF. A lateral resolution  
5 below 70 nm was evidenced in STED-SAF mode, which is similar to the results in conventional  
6 STED mode on the same sample (64 nm) (lateral resolution evaluated on 40 beads). The small loss  
7 in lateral resolution can be mainly attributed to the non-confocal detection of the STED-SAF signal.

8 In order to demonstrate the application of this STED-SAF microscope on biological samples, we  
9 imaged the microtubule network in fixed COS-7 cells immunolabeled with AF 488 (see Fig. 6). In  
10 the SAF and STED-SAF images we can clearly see surface-selective imaging of features close to  
11 the coverslip and the screening of the fluorescence from the volume. The ability of STED-SAF to  
12 efficiently remove background is particularly useful when imaging densely labeled 3D structures. In  
13 the case of biological samples, the resolution was mainly limited by the small number of photons  
14 associated with our slow acquisition and two simultaneous detection channels for true comparison.  
15 However, the introduction of faster beam-scanning mirrors could easily facilitate faster image  
16 acquisition. When imaging thick and densely labeled biological samples in STED-SAF mode, we  
17 found that the STED beam generates a substantial amount of out-of-focus background. Therefore,  
18 in that case, the SAF amplitude mask is not sufficient to efficiently reject this stray light and the use  
19 of a detection pinhole becomes necessary and significantly improves the contrast. Conversely, a  
20 very small pinhole could drastically reduce the signal. Depending on the sample, a balance between  
21 good performances in resolution and contrast with regards to collection efficiency of the signal may  
22 have to be considered. Moreover, with an adapted pinhole, we evidenced a small increase in  
23 contrast for STED-SAF compared to confocal-SAF. We can suggest that the STED beam has the  
24 ability to turn off some of the fluorescence background, which in turns enhances the SNR.

#### 1 **4. Conclusion and outlook**

2 This novel implementation gives access to membrane imaging with an axial sectioning of ~160 nm  
3 above the coverslip and effective sub-diffraction lateral resolution of 70 nm at moderate STED  
4 beam power. It could allow resolving and following dynamic events in the membrane of the cells.  
5 This instrument achieves performances similar to the previously demonstrated TIRF-STED  
6 microscope with considerably lesser experimental demands. It should be noted that SAF detection  
7 comes along with a reduction of the fluorescence signal that forms the image. Therefore, it requires  
8 optimized collection efficiency. Here, for validation purposes and true comparison, the detection  
9 was divided into a dual-view type configuration for simultaneous surface and volume imaging of  
10 the sample, which resulted in the number of detected photons to be divided by two in each path.  
11 However, the use of a flip mirror would restore the signal to its actual level and allow sequential  
12 imaging of the surface and the volume of the sample. Simultaneous dual depth imaging could also  
13 be obtained by introducing a module based on a parabolic mirror with a central hole, UAF  
14 components would be directly transmitted into one channel and SAF components reflected in the  
15 second one, allowing optimal signal detection.

16 SAF microscopy requires the samples to be embedded in a medium with a refractive index lower  
17 than the one of the glass coverslip. This refractive index mismatch induces optical aberrations,  
18 mainly spherical aberration. Usually, optical aberrations induced by imperfect coverslip thickness,  
19 inhomogeneous specimens or even temperature changes are compensated with the correction collar  
20 of the objective lens. However, it is not possible in STED microscopy because the collar adjustment  
21 deteriorates the zero of the doughnut beam. Nevertheless, it is not critical in the case of membrane  
22 imaging because the features to be imaged are not more than several tens of nanometers away from  
23 the coverslip. If necessary, image quality could be further improved by the use of adaptive optics in  
24 the detection path.

1 For a long time, the experimental complexity of STED microscopy has limited its wide adoption in  
2 the community to a small number of groups. Recent progress in the last couple of years have  
3 reduced the complexity for temporal and spatial alignment with the introduction of gated detection  
4 [25,26] and easy doughnut [27,28]. 3D-STED set-ups are also available, commercially or home-  
5 made, but the improved axial resolution comes at the cost of complex and expensive  
6 instrumentation due to the necessity of two separate STED beams for lateral (xy) and axial (z)  
7 resolution enhancement, respectively. For these reasons, our STED-SAF approach appears as an  
8 easy alternative to 3D-STED when imaging flat samples because it basically is an add-on in the  
9 detection path.

10 The proposed implementation is compatible with all STED microscopes (based on pulsed or cw  
11 lasers). Besides, this implementation relies on a one-photon-excitation architecture but is perfectly  
12 compatible with a two-photon-excitation system. In addition, this implementation was demonstrated  
13 with one color (namely green/yellow) but would also function in a multicolor STED microscope  
14 without any increase in architectural complexity in the SAF detection. The combination of these  
15 two imaging techniques offers a new tool to observe molecular phenomena on biological  
16 membranes at a nanometric scale for studying intracellular life processes. Furthermore, the demand  
17 for membrane imaging with sub-diffraction resolution is growing exponentially in many fields, and  
18 in particular in FCS-STED [29,30] and FCS-SAF [31] could be also improved with the benefits of  
19 this method (FCS-STED-SAF). We believe that ease of use of STED-SAF microscopy, could  
20 effectively open a wide dissemination of STED microscopy in cell membrane imaging/dynamic.

21

## 1 **References**

- 2 [1] J.A. Steyer, W. Almers, A real-time view of life within 100 nm of the plasma membrane, *Nat.*  
3 *Rev. Mol. Cell Biol.* 2 (2001) 268–275. doi:10.1038/35067069.
- 4 [2] D.T. Burnette, L. Shao, C. Ott, A.M. Pasapera, R.S. Fischer, M.A. Baird, C. Der Loughian, H.  
5 Delanoe-Ayari, M.J. Paszek, M.W. Davidson, E. Betzig, J. Lippincott-Schwartz, A contractile  
6 and counterbalancing adhesion system controls the 3D shape of crawling cells, *J. Cell Biol.*  
7 205 (2014) 83–96. doi:10.1083/jcb.201311104.
- 8 [3] B. Huang, M. Bates, X. Zhuang, Super-resolution fluorescence microscopy, *Annu. Rev.*  
9 *Biochem.* 78 (2009) 993–1016. doi:10.1146/annurev.biochem.77.061906.092014.
- 10 [4] S.W. Hell, Far-Field Optical Nanoscopy, *Science.* 316 (2007) 1153–1158.  
11 doi:10.1126/science.1137395.
- 12 [5] S.W. Hell, J. Wichmann, Breaking the diffraction resolution limit by stimulated emission:  
13 stimulated-emission-depletion fluorescence microscopy., *Optics Letters.* 19 (1994) 780–2.
- 14 [6] G. Vicidomini, P. Bianchini, A. Diaspro, STED super-resolved microscopy, *Nat. Methods.* 15  
15 (2018) 173–182. doi:10.1038/nmeth.4593.
- 16 [7] B. Harke, J. Keller, C.K. Ullal, V. Westphal, A. Schönle, S.W. Hell, Resolution scaling in  
17 STED microscopy, *Optics Express.* 16 (2008) 4154. doi:10.1364/OE.16.004154.
- 18 [8] B. Harke, C.K. Ullal, J. Keller, S.W. Hell, Three-dimensional nanoscopy of colloidal crystals.,  
19 *Nano Letters.* 8 (2008) 1309–13. doi:10.1021/nl073164n.
- 20 [9] M. Leutenegger, C. Ringemann, T. Lasser, S.W. Hell, C. Eggeling, Fluorescence correlation  
21 spectroscopy with a total internal reflection fluorescence STED microscope (TIRF-STED-  
22 FCS)., *Optics Express.* 20 (2012) 5243–63.
- 23 [10] T.J. Gould, J.R. Myers, J. Bewersdorf, Total internal reflection STED microscopy., *Optics*  
24 *Express.* 19 (2011) 13351–7.

- 1 [11] M. Brunstein, M. Teremetz, K. Hérault, C. Tourain, M. Oheim, Eliminating Unwanted Far-  
2 Field Excitation in Objective-Type TIRF. Part I. Identifying Sources of Nonevanescent  
3 Excitation Light, *Biophys J.* 106 (2014) 1020–1032. doi:10.1016/j.bpj.2013.12.049.
- 4 [12] D. Axelrod, Chapter 1 - Evanescent Excitation and Emission, in: A. Cornea, P.M. Conn (Eds.),  
5 *Fluorescence Microscopy*, Academic Press, Boston, 2014: pp. 1–14. doi:10.1016/B978-0-12-  
6 409513-7.00001-4.
- 7 [13] T. Ruckstuhl, J. Enderlein, S. Jung, S. Seeger, Forbidden Light Detection from Single  
8 Molecules, *Anal. Chem.* 72 (2000) 2117–2123. doi:10.1021/ac991358k.
- 9 [14] T. Ruckstuhl, D. Verdes, Supercritical angle fluorescence (SAF) microscopy., *Optics Express.*  
10 12 (2004) 4246–4254. doi:10.1364/OPEX.12.004246.
- 11 [15] T. Barroca, K. Balaa, J. Delahaye, S. Lévêque-Fort, E. Fort, Full-field supercritical angle  
12 fluorescence microscopy for live cell imaging., *Optics Letters.* 36 (2011) 3051–3053.  
13 doi:10.1364/OL.36.003051.
- 14 [16] T. Barroca, K. Balaa, S. Lévêque-Fort, E. Fort, Full-Field Near-Field Optical Microscope for  
15 Cell Imaging, *Phys. Rev. Lett.* 108 (2012) 218101. doi:10.1103/PhysRevLett.108.218101.
- 16 [17] S. Sivankutty, T. Barroca, C. Mayet, G. Dupuis, E. Fort, S. Lévêque-Fort, Confocal  
17 supercritical angle microscopy for cell membrane imaging., *Optics Letters.* 39 (2014) 555–8.  
18 doi:10.1364/OL.39.000555.
- 19 [18] N. Bourg, C. Mayet, G. Dupuis, T. Barroca, P. Bon, S. Lécart, E. Fort, S. Lévêque-Fort, Direct  
20 optical nanoscopy with axially localized detection, *Nature Photonics.* 9 (2015) 587–593.  
21 doi:10.1038/nphoton.2015.132.
- 22 [19] J. Deschamps, M. Mund, J. Ries, 3D superresolution microscopy by supercritical angle  
23 detection, *Opt. Express, OE.* 22 (2014) 29081–29091. doi:10.1364/OE.22.029081.
- 24 [20] S. Sivankutty, T. Barroca, G. Dupuis, C. Lefumeux, C. Mayet, A. Dubois, C. Marquer, S.  
25 Lécart, M.-C. Potier, E. Fort, S. Lévêque-Fort, Towards STED microscopy with nanometric

- 1 optical sectioning, in: *Single Molecule Spectroscopy and Superresolution Imaging VI*,  
2 International Society for Optics and Photonics, 2013: p. 859018. doi:10.1117/12.2004883.
- 3 [21] D. Wildanger, R. Medda, L. Kastrup, S.W. Hell, A compact STED microscope providing 3D  
4 nanoscale resolution, *J Microsc.* 236 (2009) 35–43. doi:10.1111/j.1365-2818.2009.03188.x.
- 5 [22] G. Donnert, J. Keller, R. Medda, M.A. Andrei, S.O. Rizzoli, R. Luhrmann, R. Jahn, C.  
6 Eggeling, S.W. Hell, Macromolecular-scale resolution in biological fluorescence microscopy,  
7 *Proc Natl Acad Sci U S A.* 103 (2006) 11440–11445. doi:0604965103  
8 [pii]\r10.1073/pnas.0604965103.
- 9 [23] G. Donnert, C. Eggeling, S.W. Hell, Triplet-relaxation microscopy with bunched pulsed  
10 excitation., *Photochemical & Photobiological Sciences.* 8 (2009) 481–485.  
11 doi:10.1039/b903357m.
- 12 [24] E. Fort, S. Grésillon, Surface enhanced fluorescence, *J. Phys. D: Appl. Phys.* 41 (2008)  
13 013001. doi:10.1088/0022-3727/41/1/013001.
- 14 [25] G. Vicidomini, G. Moneron, K.Y. Han, V. Westphal, H. Ta, M. Reuss, J. Engelhardt, C.  
15 Eggeling, S.W. Hell, Sharper low-power STED nanoscopy by time gating., *Nature Methods.* 8  
16 (2011) 571–3. doi:10.1038/nmeth.1624.
- 17 [26] I.C. Hernández, M. Buttafava, G. Boso, A. Diaspro, A. Tosi, G. Vicidomini, Gated STED  
18 microscopy with time-gated single-photon avalanche diode, *Biomedical Optics Express.* 6  
19 (2015) 2258. doi:10.1364/BOE.6.002258.
- 20 [27] D. Wildanger, J. Bückers, V. Westphal, S.W. Hell, L. Kastrup, A STED microscope aligned  
21 by design, *Opt Express.* 17 (2009) 16100–16110. doi:10.1364/OE.17.016100.
- 22 [28] F. Gorlitz, P. Hoyer, H. Falk, L. Kastrup, J. Engelhardt, S.W. Hell, A STED MICROSCOPE  
23 DESIGNED FOR ROUTINE BIOMEDICAL APPLICATIONS (Invited Paper), *Progress In*  
24 *Electromagnetics Research.* 147 (2014) 57–68. doi:10.2528/PIER14042708.
- 25 [29] C. Eggeling, C. Ringemann, R. Medda, G. Schwarzmann, K. Sandhoff, S. Polyakova, V.N.  
26 Belov, B. Hein, C. von Middendorff, A. Schönle, S.W. Hell, Direct observation of the

- 1 nanoscale dynamics of membrane lipids in a living cell., *Nature*. 457 (2009) 1159–62.  
2 doi:10.1038/nature07596.
- 3 [30] R. Wang, S. Brustlein, S. Mailfert, R. Fabre, M. Fallet, S. Sivankutty, H. Rigneault, D.  
4 Marguet, A straightforward STED-background corrected fitting model for unbiased STED-  
5 FCS analyses, *Methods*. 140–141 (2018) 212–222. doi:10.1016/j.ymeth.2018.02.010.
- 6 [31] J. Ries, T. Ruckstuhl, D. Verdes, P. Schwille, Supercritical angle fluorescence correlation  
7 spectroscopy, *Biophysical Journal*. 94 (2008) 221–229. doi:10.1529/biophysj.107.115998.

8

9

1 **Additional Information**

2 **Competing financial interests**

3 The authors declare no competing financial interests.

4 **Funding**

5 The authors acknowledge the ANRT, the Labex PALM and the DIM C’Nano for financial support.

6 **Acknowledgments**

7 We acknowledge the contribution of the Centre de Photonique BioMédicale to cell culture and  
8 labelling. We also acknowledge the help of Sandrine Lécart with cell culture. Finally, we thank  
9 Gaël Moneron for his help regarding STED alignment and fruitful discussions.

10 **Author contributions**

11 All the authors conceived the idea and designed the experiments. I.C.H. and G.D. prepared the  
12 biological samples with the help of Sandrine Lécart. I.C.H., S.S. and S.L.F. performed the  
13 experiments. I.C.H, S.S., G.D. and S.L.F. analyzed the data. I.C.H, S.S., G.D. and S.L.F. wrote the  
14 manuscript. All the authors read and approved the final manuscript.

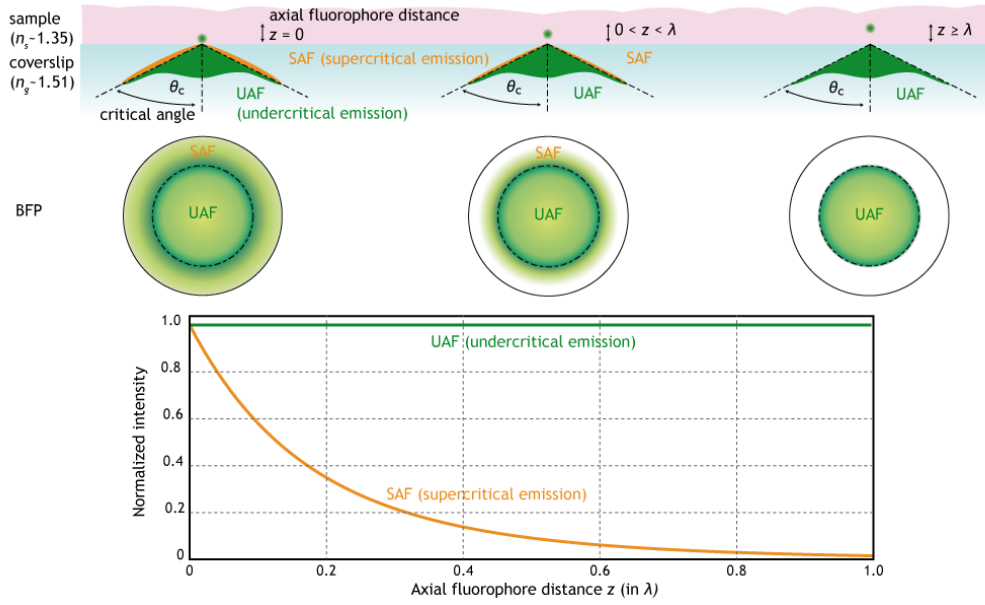
15

16

17

18

1 **Figure Legends**

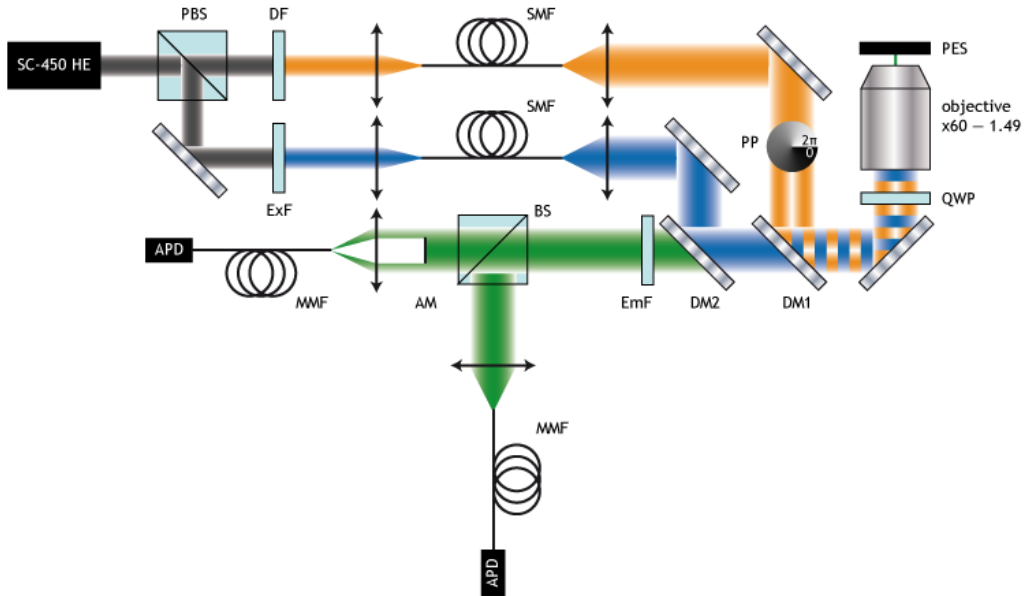


2

3 **Fig. 1. Principle of SAF emission**

4

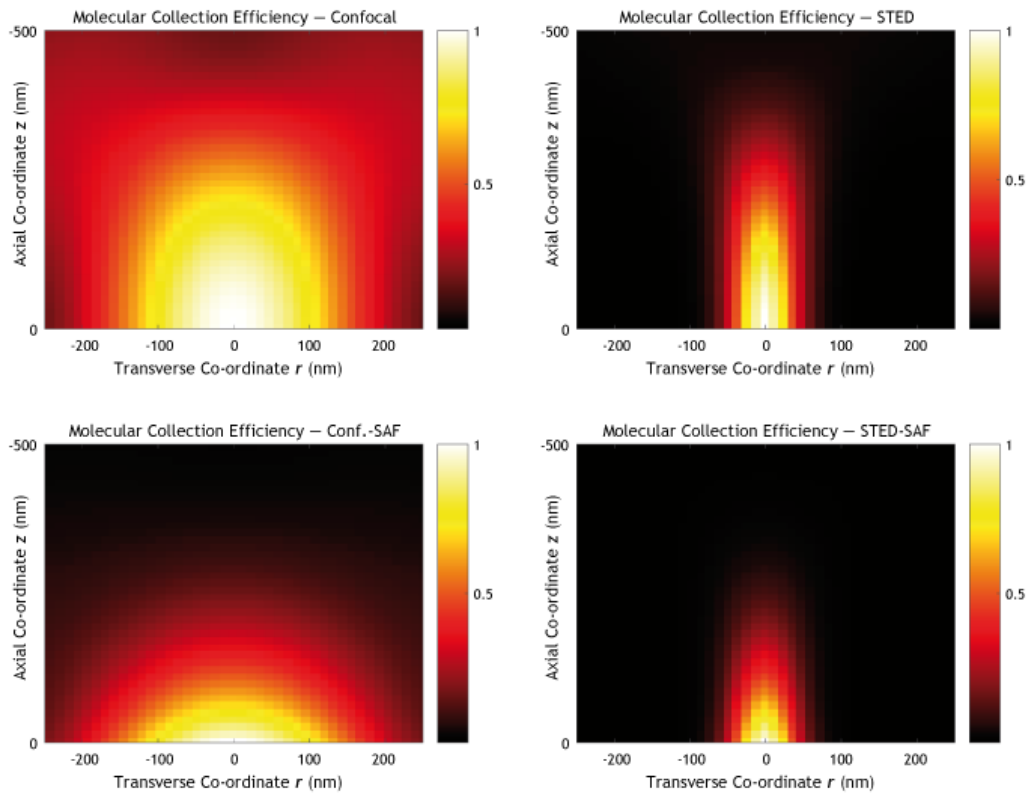
5



6

7 **Fig. 2. Experimental set-up for STED-SAF microscopy.** PBS: polarization-beam splitter; DF:  
8 bandpass depletion filter; ExF: bandpass excitation filter; SMF: single-mode fiber; PP: phase plate;  
9 DM: dichroic mirror; QWP: quarter-wave plate; PES: positioning stage scanning; EmF: emission  
10 filter; BS: beamsplitter; MMF: multi-mode fiber; AM: amplitude mask; APD: avalanche photo-  
11 diode.

12

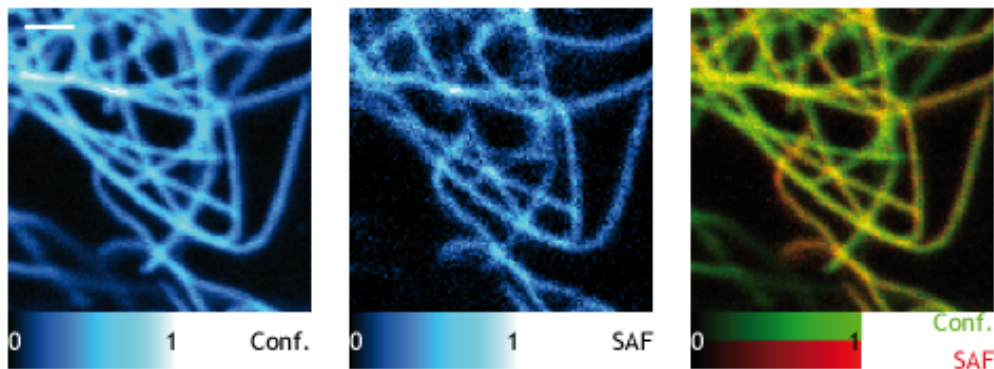


1

2 **Fig. 3. Simulation of the molecular collection efficiency (MCE) (a) Confocal (b) Confocal-SAF**  
 3 **(c) STED (d) STED-SAF**

4

5

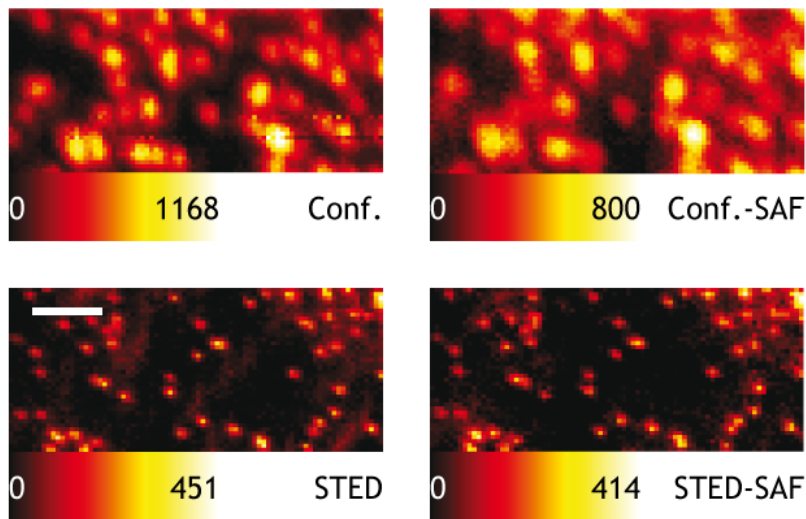


6

7 **Fig. 4. Images of microtubules labeled with Alexa 488 in COS-7 cells. (a) Confocal mode, (b)**  
 8 **Central mask-SAF mode (non-confocal detection), (c) Composite image.**

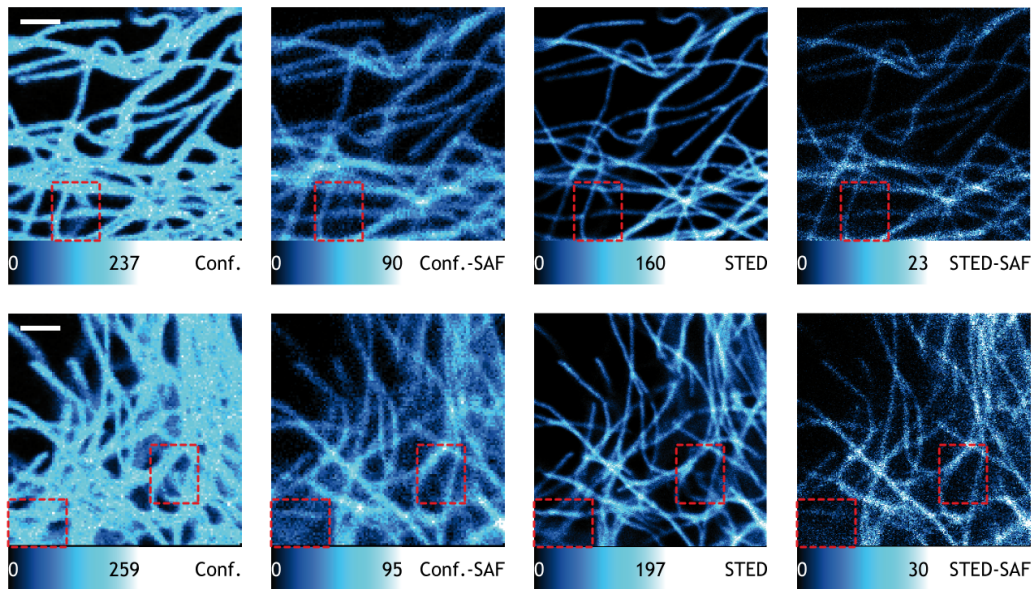
9  $P_{exc} = 10 \mu W @ 488 \pm 6 \text{ nm}$ .  $P_{STED} = 2 \text{ mW} @ 592 \pm 10 \text{ nm}$ . Pixel size 39 nm. Scale bar 1.5  $\mu m$ .

10



1  
2  
3  
4  
5  
6

**Fig. 5. Calibration sample.** Shown are confocal with STED (left panel) and SAF with STED-SAF (right panels) recordings.  $P_{exc} = 10 \mu\text{W} @ 488 \pm 6 \text{ nm}$ .  $P_{STED} = 2 \text{ mW} @ 592 \pm 10 \text{ nm}$ . Pixel size 39 nm. Scale bar 1.5  $\mu\text{m}$ .



7  
8  
9  
10

**Fig. 6. Images of the microtubule network labeled with Alexa 488 in COS-7 cells.**  $P_{exc} = 10 \mu\text{W} @ 488 \pm 6 \text{ nm}$ .  $P_{STED} = 2 \text{ mW} @ 592 \pm 10 \text{ nm}$ . Pixel size 39 nm. Scale bar 1.5  $\mu\text{m}$ .